Characterisation of soft tissue viscous and elastic properties using ultrasound elastography and rheological models: Validation and applications in plantar soft tissue assessment

Aldo Tecse[1], Stefano E Romero[2], Roozbeh Naemi[3] and Benjamin Castaneda[4]
Accepted Manuscript online 30 March 2023 •

Author affiliations
[1] Engineering, Pontificia Universidad Catolica del Peru, 1801 Universitaria Avenue, San Miguel, Lima, Lima, Lima, 15038, PERU
[2] Pontificia Universidad Catolica del Peru, 1801 Universitaria Avenue, Lima, Lima, 15088, PERU
[3] Centre for Biomechanics and Rehabilitation Technologies, Staffordshire University, College Rd, Stoke-on-Trent, Staffordshire, ST4 2DE, UK
[4] Department of Engineering, Pontificia Universidad Catolica del Peru, Av. Universitaria 1801, San Miguel, Lima 32-Perú, Lima, 32, PERU

Received 19 October 2022
Revised 6 March 2023
Accepted 30 March 2023

Abstract

Objective: The mechanical behaviour of soft tissue is influenced by its elastic and viscous characteristics. Therefore, the aim of this study was to develop a protocol to characterise the viscoelastic properties of soft tissues based on ultrasound elastography data. **Approach:** Plantar soft tissue was chosen as the tissue of interest, and gelatine-phantoms replicating its mechanical properties were manufactured for validation of the protocol. Both plantar soft tissue and the phantom were scanned using Reverberant shear wave elastography at 400-600 Hz. Shear wave speed (SWS) was estimated using the US particle velocity data. The viscoelastic parameters were extracted by fitting the shear wave dispersion data to the Young's modulus as a function of frequency derived from the constitutive equations of the eight rheological models (four classic and their fractional-derivative versions). Furthermore, stress-time functions derived from the eight rheological models were fitted to the phantom stress-relaxation data. **Main results:** The viscoelastic parameters estimated using elastography data based on the fractional-derivative (FD) models were closer to those quantified using the mechanical test. In addition, the FD-Maxwell and FD-Kelvin-Voigt models can more effectively replicate the viscoelastic behaviour of the plantar soft tissue with minimum number of model parameters (R^2 = 0.72 for both models) . Hence the FD-KV and FD-Maxwell models can more effectively quantify the viscoelastic characteristics of the soft tissue compared to other models. **Significance:** In this study, a method for mechanical characterisation of the viscoelastic properties of soft tissue in ultrasound elastography was developed and validated. An investigation into the most valid rheological model and its applications in plantar soft tissue assessment were also presented. This approach for the characterisation of viscous and elastic mechanical properties of soft tissue has implications in assessing the soft tissue function where those can be used as markers for diagnosis or prognosis of tissue status.

Keywords: elastography, plantar soft tissue, shear waves, ultrasound, viscoelasticity

1. Introduction

The behaviour of soft tissue under a load is governed by its mechanical characteristics. These mechanical characteristics can be used to assess the health and function of the tissues. Medical imaging has been used to assess the mechanical properties of soft tissue for more than 30 years. Initially, elastography was described as a set of techniques focused on estimating the modulus of elasticity or a related parameter, such as the shear wave speed (SWS) (Huang and Zheng, 2015; Ormachea and Parker, 2020). However, this modulus, also known as Young's modulus, reflects a combination of elastic and viscous properties (Parker *et al.*, 2018; Zhang *et al.*, 2008). While the elastic properties represent the resistance of tissue to deformation, the viscous component represents its resistance dependent on the deformation rate. Hence, the Young's modulus of a tissue can be changed by varying combination of viscous and elastic characteristics or just one of them (Parker *et al.*, 2018; Murakami *et al.*, 2015).

Soft tissue exhibits viscoelastic behaviour under load; hence, to quantify the true nature of tissue biomechanical behaviour, both viscous and elastic characteristics need to be considered. A more detailed overview of the estimation of viscoelastic properties can provide further understanding of the mechanical behaviour of tissues, with implications for the diagnosis and evaluation of treatments on the mechanical properties of soft tissues. It has been previously established that the characterization of viscoelasticity could be helpful for pathologies such as cancer (Zhang *et al.*, 2008; Ormachea *et al.*, 2019), fibrosis associated with liver cirrhosis (Ormachea and Parker, 2020; Murakami *et al.*, 2015; Ormachea *et al.*, 2019; Miyake *et al.*, 2019), fatty liver (Murakami *et al.*, 2015), diabetes (Negishi *et al.*, 2020; Roozbeh *et al.*, 2016; Naemi *et al.*, 2017; Naemi *et al.*, 2021; Hsu *et al.*, 2007; Chao *et al.*, 2011), and atheroma (Ormachea and Parker, 2020). Furthermore, characterisation of viscoelastic parameters can aid computational modelling, which provides further insight into the biomechanics of the tissue (Negishi *et al.*, 2020). In addition, understanding these properties may allow the development of improved therapeutic products and interventions (Suzuki *et al.*, 2017).

Several constitutive viscoelastic models have been developed to characterise biomechanical properties (Zhou and Zhang, 2018). Constitutive equations relate the stress and deformation of a tissue to a stimulus. Young's modulus is defined as the ratio between the stress and strain. Shear wave elastography can quantify the modulus of elasticity at various frequencies (Zhang *et al.*, 2007). Therefore, by performing a frequency transformation, the viscoelastic properties can be related to Young's modulus (Zhou and Zhang, 2018; Ormachea *et al.*, 2018). In addition, the mechanical properties that were quantified using the elastography technique can be validated by comparing them with the properties that can be extracted from mechanical tests of the specimen such as stress relaxation. In stress relaxation tests, the temporal stress response of the material is fitted with the stress-time function derived from each mechanical model to quantify the viscoelastic parameters (Zhang *et al.*, 2007; Zvietcovich *et al.*, 2017; Zhang *et al.*, 2018).

The early developed models were linear and combined purely viscous and elastic elements (Zhang *et al.*, 2021). These models have been used to characterise the biomechanical properties of soft tissues in the past using small strain responses when the tissue was subject to 5% strains (Parker *et al.*, 2018; Zvietcovich *et al.*, 2017). Linear viscoelastic constitutive equations can be expressed by differential equations relating the stress and strain responses, and their temporal derivatives. Although classical models predict a strong frequency dependence of damping properties, measurements of viscoelastic materials reveal a very small change in their dissipative behaviour with varying frequencies (Jones, 2001; Schmidt and Gaul, 2008). Thus, a generalisation of the classical viscoelastic models was subsequently performed using fractional derivatives instead of integer-order derivatives (Schmidt and Gaul, 2008). This results in greater freedom of the classical models and a better relationship between these models has been previously reported (Parker *et al.*, 2019).

The mechanical properties of different tissues have been characterised using various techniques (Ormachea and Parker, 2020). Recently, tissues adjacent to the first metatarsal head, third metatarsal head (3-MTH), and calcaneus have been characterised using reverberant shear wave elastography (RSWE) technique (Romero *et al.*, 2022). This technique differs from others because it takes advantage of the bounces generated by inhomogeneities, bones, and organ boundaries (Parker *et al.*, 2017). For example, artefacts have been reported using acoustic radiation force-based techniques for soft plantar tissues (Lin *et al.*, 2017). These artefacts affect the robustness of viscoelasticity estimations using the frequency characteristics (Miyake *et al.*, 2019).

One of the tissues that can benefit from the characterisation of biomechanical properties is plantar soft tissue (Naemi *et al.*, 2022). Plantar soft tissue is important in terms of its mechanical function, as it regulates ground reaction forces during locomotion (Cavanagh *et al.*, 2000). Understanding the mechanical properties of plantar soft tissue is particularly important for assessing the risk of injury, as it has been shown that diabetic patients with wounds, infections, or ulcerations of the foot are at an increased risk of amputation (Naemi *et al.*, 2022; Romero *et al.*, 2022). Therefore, the purpose of this study is to develop a method for the mechanical characterisation of the viscoelastic properties of soft tissue using ultrasound elastography. In doing so, eight rheological models, including classical biomechanical models and their fractional derivative (FD) extensions, were investigated and the validity and applicability of each model were explored.

2. Method

Figure 1 shows the steps followed in the study. In the first step, (a) shows the SWS profile reported using the RSWE technique in five patients (Romero *et al.*, 2022). Then, in Figure 1 (b), phantoms were manufactured by changing the concentration and the one with SWS in the range of plantar soft tissue was chosen. In Figure 1 (c), for each rheological model, the time domain stress response was developed to estimate the viscoelastic properties from mechanical measurements. In addition, the theoretical SWS in the frequency domain was derived to extract viscoelastic properties from the measured SWS. Subsequently, in Figure 1 (d) and (e), a curve-fitting process is performed simultaneously in the time and frequency domains for the eight rheological models. The process is presented for the equations in Table I for the Standard Linear (SL) and FD-SL models (Lin, 2020). In Figure 1 (f), the rheological models were validated by contrasting the viscoelastic properties obtained from the mechanical measurements and SWS.

Finally, Figure 1 (g) shows the estimation of viscoelastic properties in plantar tissue using validated rheological models from the SWS reported in the literature.

2.1. Phantom Manufacturing and RSWE experiments

Using the SWS profile reported in the tissue adjacent to 3 MTH by Romero with the RSWE technique (Romero *et al.*, 2022), we sought to manufacture a gelatine phantom with similar SWS values through frequency (Figure 1 (a)). For this purpose, four custom-made phantoms of 2 L volume were prepared with gelatine concentrations of 6%, 8%, 10% and 12%. The manufacturing proportions and materials are detailed in Section 1 of the Supplementary information. Then, RSWE experiments were performed to characterise the SWS of each phantom and determine which one has the SWS closest to that reported by Romero et al (Romero *et al.*, 2022), see Fig 1 (b).

Reverberant fields were generated by multifrequency vibrations between 400 and 600 Hz with steps of 50 Hz using two external speakers (Misco, Pleasanton, CA, USA), as shown in Figure 2 (b). Three repetitions were performed for each experiment, and the displacement data was extracted using the linear array L11-4v (Central frequency of 9 MHz) operated by the Vantage 64LE (Verasonics, Kirkland, WA, USA) ultrasound system, Fig. 2 (c) and (g). An ultrasound gel pad was used because better results were obtained when using the RSWE technique (Naemi *et al.*, 2022), as shown in Figure 2 (f). Supplementary Figure 1 shows that the phantom made with 8% gelatine concentration is the most similar to the SWS-frequency profile of the plantar soft tissue (Naemi *et al.*, 2022; Romero *et al.*, 2022). Thus, a validation analysis of the viscoelasticity parameters using mechanical measurements was performed for the phantom with this concentration, see Figure 2 (d). To this end, from this point all the experiments and references to phantom will refer to the phantom of 8% concentration of gelatine.

2.2. Estimation of SWS

To estimate SWS, the particle velocity was first reconstructed from the recorded data. Time-frequency filters were then applied to separate the frequencies of interest. In addition, a spatial bandpass filter was applied to reduce the noise. Subsequently, Fourier transform was applied in the time domain for each filtered frequency. Using the magnitude and phase, a 2D auto-correlation was performed. The profile of this complex autocorrelation can be expressed as a combination of Bessel functions on wavenumber (k) (Zvietcovich *et al.*, 2019).

$$B_{v_z v_z}(\Delta t, \Delta\varepsilon_x) = V_{RMS}^2 cos\,(\omega_0 \Delta t)\left[\frac{j_0(k\Delta\varepsilon_x)}{2} - \frac{j_1(k\Delta\varepsilon_x)}{2k\Delta\varepsilon_x}\right] \quad (1)$$

where $B_{v_z v_z}$ is the normalised 2-D autocorrelation, Δt is the time-difference, $\Delta\varepsilon_x$ is the displacement along the x-axis, ω_0 is the angular vibration frequency, $V_{RMS}^2 cos\,(\omega_0 \Delta t)$ is the real part of the squared particle velocity magnitude, j_0 and j_1 are the spherical Bessel functions of the zeroth and first order, respectively, and k is the local wavenumber. Equation (1) was used to estimate the wavenumber via least-squares regression analysis. Finally, the SWS was determined from the estimated wavenumber (k^*) using Equation (2).

$$SWS = \frac{2\pi f}{k^*} \quad (2)$$

An elastogram was formed by estimating the SWS for each data point. To preserve the most reliable estimations, a threshold of 0.7 for the coefficient of determination was used on the elastogram similar to Romero's work (Romero *et al.*, 2022). Only these values were used to obtain the mean SWS to estimate viscoelastic properties.

2.3. Rheological models for the characterisation of viscoelastic properties

The RSWE technique allows the SWS to be obtained at different frequencies. The SWS is related to Young's modulus using Equation (3).

$$SWS(f) = \sqrt{\frac{E(f)^*}{3\rho}} \quad (3)$$

where $E(f)^*$ is the frequency-dependent Young's modulus and ρ is the density of the material. Taking the constitutive equations, Young's modulus can be developed using Equation (4).

$$E_z{}^* = \frac{\sigma_z}{\varepsilon_z} \quad (4)$$

where σ and ε are the stress and strain of the material, respectively, in the frequency domain. In Table I, s is the Laplace transform variable that can be replaced by $i2\pi f$ to relate these equations to the vibration frequency used for SWS acquisition using RSWE technique. The viscoelastic parameters were then estimated using a curve-fitting process on the SWS averages for each frequency. This process corresponds to Figure 1 (e).

Characterisation of the viscoelastic properties of plantar soft tissue was performed using SWS extracted from tissue adjacent to the 3-MTH of five healthy volunteers. On the other hand, the viscoelastic properties of the phantom were extracted using the shear wave dispersion estimated in this study. The same acquisition and processing protocol was followed for the estimation of SWS in the phantoms and plantar soft tissue (Romero *et al.*, 2022). The SWS averages of the region-of-interest (ROI) of three experiments were used for each frequency. Thus, fifteen SWS averages were used to estimate the parameters of each model. The real part of the Young's modulus equations in Table I was used in combination with Equation (3) to determine the relationship between the SWS and viscoelastic parameters of each model. The limits of all parameters were restricted to positive values.

2.4. *Estimation of viscoelastic properties using Mechanical Measurements*

The stress-relaxation response is obtained when a step constant strain is applied. This deformation first generates an abrupt increase in stress (Stress segment). However, then the stress decreases (relaxation segment) owing to the viscosity of the material.

Using the time-domain constitutive equations of the models listed in Table I, the theoretical stress function response can be determined. To do this, a constant step input in the Laplace domain is applied to the system (constitutive equation). Subsequently, inverse Laplace transform was applied to obtain the time-domain response. For fractional-derivative models, the inverse transform requires the use of the Mittag-Leffler function (F_α) (Schmidt and Gaul, 2008; Kexue and Jigen, 2011).

$$F_\alpha = \sum_{k=0}^{\infty} \frac{x^k}{\Gamma(\alpha k+1)} \quad (5)$$

Stress relaxation tests were performed on three cylindrical samples extracted from the phantom using a coring-knife with a height of 30 mm and diameter of 31 mm made with the same mixture used to construct the 8% gelatine-phantom (Zhang *et al.*, 2007; Ormachea *et al.*, 2016).

The mechanical properties of the samples were evaluated using a universal mechanical testing machine (Z0.50, Zwick/Roell, Ulm, Germany) equipped with a 10 N load cell. The compression rate was set to 0.5 mm/s and the strain value was set to 5%. The duration of the tests was approximately 700 seconds. The relaxation segment of the data was subsequently analysed by fitting a curve-fitting algorithm to the stress response $G(t)$ equations outlined in Table I. This process was used to estimate the viscoelastic properties of the phantom as shown in Figure 1 (d) through mechanical measurements. The average of the stress data from three experiments was used for the fitting, with stress data for each experiment being presented in Supplementary Figure 2.

3. Results

3.1. *Estimation of the viscoelastic properties in the phantom experiments*

Figure 3 shows the shear wave dispersion data fitted to the eight theoretical models, shown in Table I. First, the biomechanical parameters of each model were recovered. The SWS information was then reconstructed for a broader range of frequencies (0 to 650 Hz) using the estimated parameters, see coloured lines in Figure 3.

The coefficients of determination for the phantom experiment (R^2_{Ph}) are also shown in Figure 3. The values of R^2_{Ph} of the classical models are slightly larger than those of their fractional-derivative versions, except for the KV model. The reconstructed phase velocity decreases at lower frequencies which is expected from a viscoelastic material. However, only the Maxwell model reaches 0 m/s given that this model is contrained by its equation, see the Young's modulus of this model in Table I. Finally, Table II shows the viscoelastic parameters estimated for all the models on the phantom experiment.

3.2. *Validation of phantom viscoelastic properties measurements*

The results of the stress-relaxation experiments on the phantom are presented in Figure 4, which shows the fitted curves of the fractional-derivative versions of the models. This is because only these models were able to accurately fit the collected data. In contrast, the classical models (such as the KV and Maxwell models) exhibited a non-asymptotic response represented by a horizontal line at a constant stress value, which was not observed in the collected data. As a result, the curve-fitting of these classical models did not accurately reflect the behaviour of the material, and their results are not included in the presentation.

The estimated biomechanical parameters were then used to predict SWS and compare the results with information obtained using RSWE in a manner similar to Zvietcovich *et al.*, see Figure 5 (Zvietcovich *et al.*, 2017).

3.3. Estimation of the viscoelastic properties in the plantar soft tissue in-vivo experiments

Similar to the phantom, the average SWS of each volunteer at the 3-MTH ROI was retrieved from three trials for each foot. Figure 6 shows the fitted curves for the classical models and their fractional derivatives version for one volunteer. Again, the biomechanical parameters of each model were recovered. Then, the phase velocity was reconstructed for a broader range of frequencies (0 to 650 Hz) using the estimated parameters, see coloured lines in Figure 6.

Figure 7 presents a summary of the R_V^2 (coefficient of determination for volunteers SWS data) values for all the models, as evaluated for the five volunteers. The R_P^2 (coefficient of determination for phantom SWS data) values from Figure 3 are also included for comparative purposes. It is expected that the R_P^2 values, which are derived from the phantom experiment, would be higher than the median values of R_V^2 for all the models. This is the case for all models except for the FD-SLS model, where the R_P^2 value is lower than the median value, but still close to it.

It is observed in Figure 7 that similar median values above 0.7 were obtained for the KV, FD-KV, FD-Maxwell and FD-SL models. In contrast, the Maxwell, SL, SLS, and FD-SLS models exhibit median values below 0.55. Notably, the FD-SLS model yielded a particularly low value for both the phantom and in-vivo data.

Table III summarises the biomechanical parameters estimated in the trials of the five volunteers. A dash is used when the parameters are not included in the biomechanical model. The values of α are in a range between 0.2 and 0.5 for all models. This implies that the fractional element tends to behave more as a spring than as a dashpot for all the fractional derivative models. That is why the values if we compare the values of μ_α with the ones of η between the classical and fractional derivative versions, we observe that they differ and represent a different range. The top panel of Fig. 8 shows a narrow range of values for μ_0 obtained for KV, FD-KV, and FD-SL models, in contrast to the SL, SLS, and FD-SLS which showed a lower value of coefficient of determination. Similarly, the bottom panel shows a narrow range of μ_1 values for Maxwell, FD-Maxwell, and SL models.

In addition, the purely viscous and viscoelastic parameters estimated with the SWS measurement between the phantom and plantar soft tissue of the 3-MTH tissue were compared in Supplementary Figure 4, 5, and 6. All the values of the viscoelastic properties of the phantom are within the range of those estimated for the 5 healthy volunteers, see Figure 8, Supplementary Figure 4, 5, and 6.

Similar values for the order of the fractional-derivative (α) were also found between the phantom and plantar soft tissue at 3-MTH. The value for the FD-KV model was near 0.6 in the lower range of values for the phantom. The difference in the viscous and viscoelastic parameters is explained by the manufacturing of the phantom, given that no castor oil was used.

4. Discussion

In general, high values of R_P^2 (>0.7) were obtained for all models during the characterization of the biomechanical parameters of the phantom, with the exception of the FD-SLS model. However, when evaluating healthy volunteers, the KV, FD-KV, FD-Maxwell and FD-SL models exhibited higher median values of R_V^2 (>0.7).

Moreover, the classical models did not provide an adequate fit to the stress relaxation data and were not able to represent the behaviour of the phantom during mechanical tests. The results of this study are in line with previous research that indicated that the simplicity of classical models does not adequately represent stress-relaxation behaviours (Murakami *et al.*, 2015; Poul *et al.*, 2022). Our results on the superiority of fractional derivative models for mechanical validation are in line with several studies using the stress-relaxation test utilising fractional-derivative models (Parker *et al.*, 2018; Zvietcovich *et al.*, 2017; Parker *et al.*, 2019; Craiem *et al.*, 2008).

Hence, the values of η and μ_α from classical models and their fractional derivative versions, respectively, are not equal (Poul *et al.*, 2022). Furthermore, there are parameters that reach extreme values which seem to fall outside the physiological range. For instance, Table III shows that the upper limit of μ_1 reach extreme values for one patient using the SLS, SL, and FD-SL models. However, these values could be explained by equations in Table I, where there is a complex interaction among the elastic parameters, such as divisions and not necessarily just addition and multiplication. Nonetheless, the theoretical responses of the classical models are not close to the data obtained during the stress relaxation tests, which we can notice by examining the stress responses in Table I and Fig. 4. Therefore, fractional-derivative models are more suitable for understanding and relating these two phenomena (Parker *et al.*, 2019).

Except for the classical models that obtain a higher value of R_V^2 given that they were unable to characterize the stress relaxation experiment, the FD-KV, FD-Maxwell, and FD-SL models show a higher median R_V^2 value than other models. However, FD-KV and FD-Maxwell provide a more consistent range of parameters than FD-SL, see the bottom panel in Figure 8.

Besides, both the FD-KV and FD-Maxwell models require fewer parameters than the FD-SL model. Supplementary Figure 7 illustrates the adjusted R_V^2 values, which take into account the number of parameters fitted for each model. This figure demonstrates that both the FD-KV and FD-Maxwell models maintained a median adjusted R_V^2 value above 0.5. In particular, the FD-KV model had a value above 0.6 which is in agreement with previous study (Poul et al., 2022). As such, FD-KV and FD-Maxwell models are better suited for characterizing the viscoelastic properties of plantar soft tissue while reducing the number of parameters or the degrees of freedom required by the model.

The heel pad consists of a fatty tissue cushion along with a structure constituting two distinct regions. This includes a layer containing a stiffer microchamber and deeper layer of relatively compliant macrochambers (Roozbeh *et al.*, 2016; Naemi and Chockalingam, 2013). Hence, the fractional derivative models in which the fractional derivative element allows liberty may better replicate the complex structure and distribution of the plantar soft tissue and its mechanical behaviour.

The viscoelastic behaviour of the plantar tissue was successfully replicated using the manufactured phantom, please see Figure 8, Supplementary Figures 4, 5, and 6 and Tables II and III. This is evidenced by the finding that the elastic properties estimated for the phantom were within the IQR of the values estimated for plantar soft tissue. Also, the estimated values for the viscous/viscoelastic properties of the phantom are inside the plantar soft tissue ranges. This is consistent with our expectations because even though the phantom was chosen such that the estimated SWS of the phantom was close to that of the foot, no purely viscous substance was used for phantom manufacture. Overall, it appears that the proposed phantom behaviour matched the viscoelastic characteristics of the plantar soft tissue and its mechanical behaviour (Naemi and Chockalingam, 2013).

Previously, phantoms have been manufactured with different amounts of castor oil to modify their viscosity (Parker *et al.*, 2018). However, the manufacturing of these phantoms is based on the idea of viscous capsules inside the phantom that replicate the large intracytoplasmic lipid vacuoles present in liver tissue. In contrast to the liver, plantar soft tissue has a different function and may not exhibit this phenomenon.

The shear wave dispersion data of the phantom used in our study is in line with the results reported in Zvietcovich for elastic phantoms of 10% and 15% concentration that were reported as 3.11 m/s and 4.78 m/s, respectively (Zvietcovich *et al.*, 2017).

Additionally, the viscoelastic parameters reported by Zhou and Zhang for a phantom fall within the interquartile range of our results for the volunteers and are also consistent with our phantom results for the KV, Maxwell, and SLS models (Zhou and Zhang, 2018). The only exception is the FD-KV model, where Zhou and Zhang obtained a different value of α (α = 1.00). This discrepancy may be since their study only involved fitting the model to data from a single experiment over a frequency range of 100 to 240 Hz. The other models investigated in our study were not considered in their research, hence no direct comparisons could be made. Likewise, Poul *et al.* performed a study with a similar approach to characterize *ex vivo* bovine liver tissues. In this case our value of α estimated for plantar soft tissue with the FD-KV model is found to be close to 0.2 (Poul *et al.*, 2022).

A significant difference in the estimated value for μ_0 is observed between the KV and FD-KV models. This discrepancy may be attributed to the fact that the KV model employs the magnitude of the complex Young's modulus, while the FD-KV model and other models use the real part. Furthermore, previous studies have demonstrated that at high frequencies (>100 Hz), the frequency-independent term (μ_0) can be considered negligible for the FD-KV model (Parker *et al.*, 2019; Zhang *et al.*, 2007; Ormachea *et al.*, 2018; Poul *et al.*, 2022). Additionally, the frequency range used for the phantom experiments was chosen based on the data from in vivo studies of plantar soft tissue (Romero *et al.*, 2022; Naemi *et al.*, 2022). Other studies have used higher frequency ranges when assessing characteristics of tissues other than plantar soft tissue (Ormachea *et al.*, 2016; Kiss *et al.*, 2004; Chen *et al.*, 2004). As such, those are considered out of the scope of the present study and to use the models in other tissue and across a different frequency range further validation may be required.

Conventional values for compression rate (0.5 mm/s) and strain (5%) were chosen based on the literature (Parker *et al.*, 2019; Parker *et al.*, 2018; Zvietcovich *et al.*, 2017; Poul *et al.*, 2022). However, the differences found between the estimated parameters in the time and frequency domains can be explained by the dependency of the stress-relaxation tests. The results of these tests depend on the initial indentation rate and are sensitive to the loading process (Murakami *et al.*, 2015; Negishi *et al.*, 2020). Therefore, future mechanical tests that better replicate soft tissue deformation during weightbearing activities of daily living may be more useful (Naemi and Chockalingam, 2013; Naemi *et al.*, 2016; Behforootan *et al.*, 2017).

Previous literature studies have highlighted the importance of characterising the biomechanical properties of different body tissues (Parker *et al.*, 2019; Romero *et al.*, 2022). This study is the first to develop and validate a method for quantifying the viscoelastic properties of plantar soft tissue based on ultrasound elastography. These parameters can have implications in understanding the behaviour of tissues under load and in diagnosing their malfunction in disease conditions.

The method proposed in this study is fully validated for characterisation of plantar soft tissue across relevant frequencies. Further validation in future studies is required for using the method across a different frequency range or when the characterisation of a different tissue of interest is intended.

5. Conclusion

In this study, a method for the mechanical characterization of the viscoelastic properties of soft tissue using ultrasound elastography was developed and validated. The study also explored the most appropriate rheological model and its applications in the assessment of plantar soft tissue. The viscoelastic properties of the soft plantar tissue adjacent to the 3-MTH of five healthy volunteers were selected as the target tissue. The proposed method of characterization was validated using a custom-made phantom that replicated the shear wave dispersion data reported for 3-MTH in the literature. The results of this study provide a valuable tool for the non-invasive evaluation of the viscoelastic properties of soft tissue, specifically in the context of the plantar soft tissue.

The validation of the viscoelastic properties was based on fitting a curve represented by the mechanical behaviour of each of the eight rheological models to the shear wave dispersion data of the manufactured phantom. For this purpose, this study developed the stress $[G(t)]$ response and the complex Young's modulus $E^*(f)$ equations for each model. It should be noted that in this study, the time and frequency responses of the SL and FD-SL models were introduced for the first time. Stress response equations were used to characterise the viscoelastic properties from the mechanical measurements, while Young's modulus equations were used to extract the viscoelastic properties of the shear wave dispersion data. Then, the validation of the protocol to characterise the viscoelastic properties was performed by comparing the estimates from the mechanical measurements against the SWS measurements. Although this protocol was implemented using plantar soft tissue as the tissue of interest, the same approach can be applied to characterise the mechanical characteristics of other tissues.

The results of this study indicate that classical models are inadequate for characterizing the stress response when compared to fractional-derivative models. Specifically, the FD-KV and FD-Maxwell models were found to have the highest median values of the coefficient of determination while maintaining consistent measurements for the phantom and volunteers across all variables. Additionally, FD-KV and FD-Maxwell models maintained a higher coefficient of determination even when normalized to the number of variables, in contrast to the FD-SL model, which has one more variable. Therefore, the FD-KV and FD-Maxwell models can quantify the viscoelastic characteristics of the soft tissue with minimum number of model parameters.

In conclusion the FD-KV and FD-Maxwell models are more suitable for characterizing the viscoelastic properties of plantar soft tissue under conditions commonly encountered in elastography.

Figures

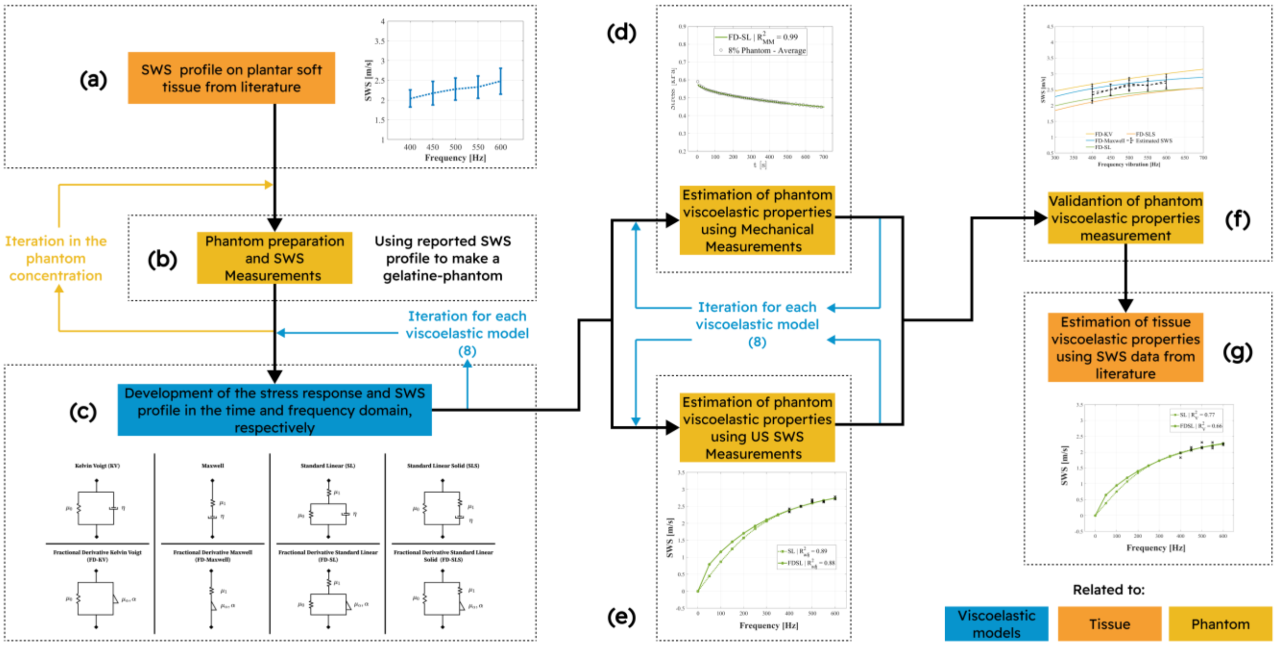

Figure 1. Methodology followed to estimate the viscoelastic properties of 3-MTH and validation of the method in phantoms. Panel (a) shows the shear wave dispersion data reported in literature. Panel (b) represents the iterative process to replicate data in Panel (a) with custom-made phantoms. Panel (c) represents the four classical rheological models and their fractional-derivative versions compared in this study (Eight models in total). Panels (d), (e) and (g) show the process for the Standard Linear (SL) and FD-SL models using their equations shown in Table I. Panel (f) shows the reconstruction of the SWS using Young

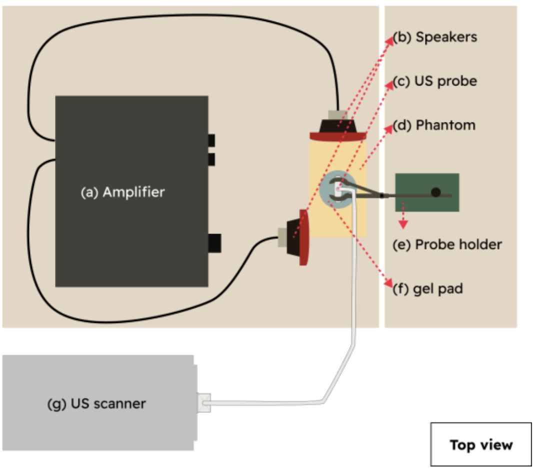

Figure 2. Top view of the custom setup that was implemented for the acquisition of US data from the phantoms. In addition to the tools and equipment listed in the figure, a computer was used to send the vibration signal to the amplifier (a) and display the B-mode during acquisition. A different desk was used to position the transducer holder (e) so that vibrations do not directly affect the transducer.

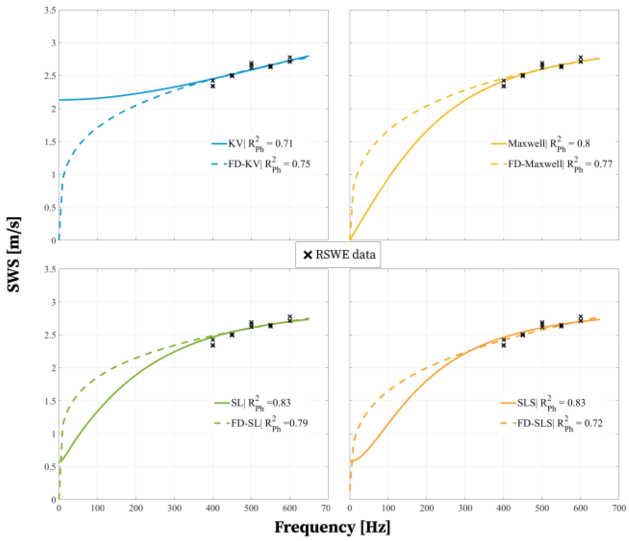

Figure 3. Fitted curves for classical models and their fractional-derivative extensions. The models were fitted to the SWS of the 8% concentration phantom. The coefficients of determination (R_{Ph}^2) for the experiments in the phantom are shown.

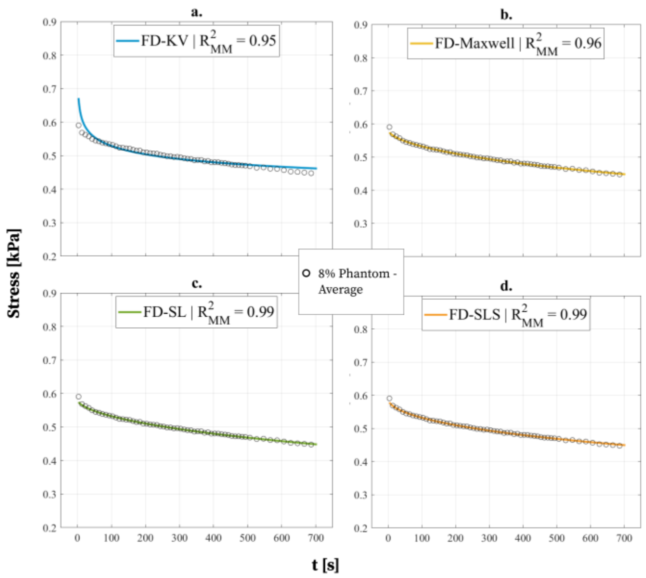

Figure 4. The panels show the fractional-derivative models fitted to the stress-relaxation data of the 8% concentration phantom. The coefficients of determination (R^2_{MM}) for the mechanical measurements in the phantom are also shown.

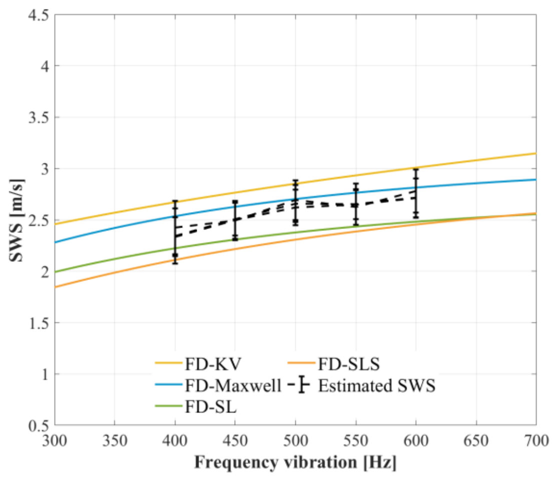

Figure 5. The panels show the fractional-derivative models fitted to the stress-relaxation data of the 8% concentration phantom. The coefficients of determination (R^2_{MM}) for the mechanical measurements in the phantom are also shown.

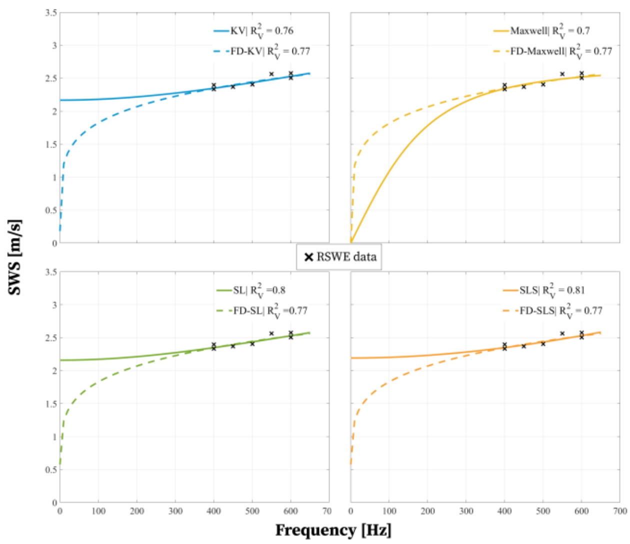

Figure 6. Fitted curve for classical models and their fractional-derivative version. The curves were fitted to the SWS speed measurements in the 3-MTH of the left foot of one of the volunteers. The coefficients of determination (R^2_V) for the in-vivo experiments are shown.

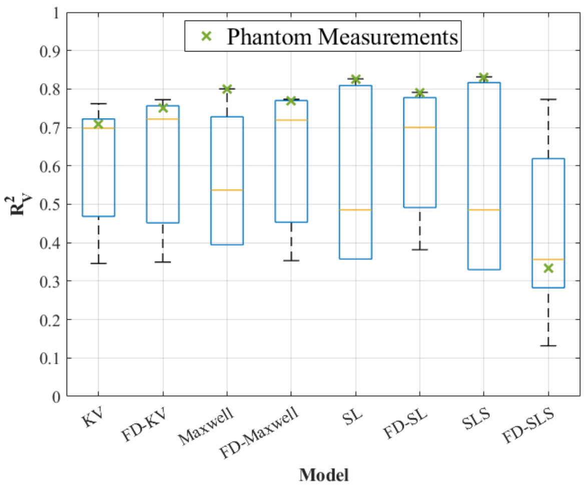

Figure 7. Distribution of the coefficient of determination (R^2_V) for the in-vivo experiments for each model. The yellow mark indicates the median, and the bottom and top edges of the blue box indicate the 25th and 75th percentiles, respectively. The whiskers extend to the most extreme data points not considered outliers.

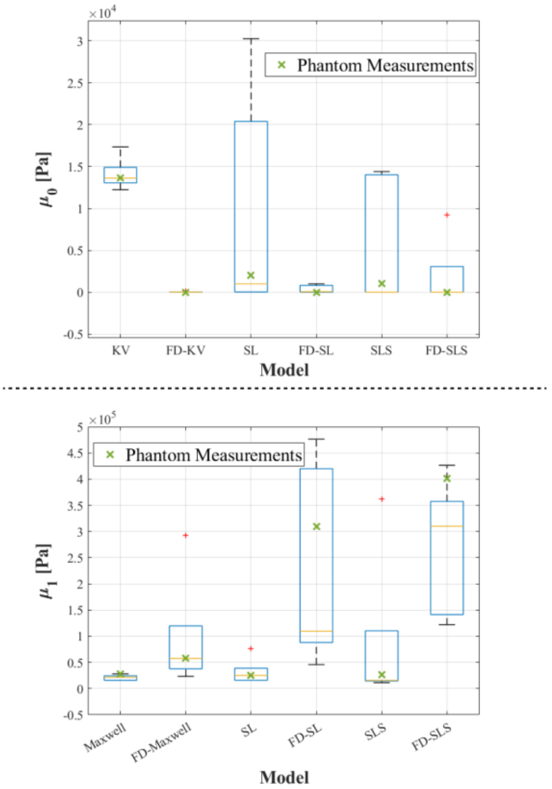

Figure 8. Comparison between the elastic properties of the plantar soft tissue and elastic properties estimated in the phantom for each model. The outliers are plotted individually in red.

Tables

TABLE I
YOUNG'S MODULUS AND STRESS RESPONSE OF KELVIN-VOIGT (KV), MAXWELL, STANDARD LINEAR (SL), STANDARD LINEAR SOLID (SLS), AND THEIR FRACTIONAL DERIVATIVE (FD) VERSIONS.

Model	Stress response	Young's Modulus
KV	$\mu_0 + \eta\delta(t)$	$\mu_0 + (i2\pi f)\eta$
FD-KV	$\mu_0 + \dfrac{\mu_\alpha t^{-\alpha}}{\Gamma(1-\alpha)}$	$\mu_0 + (i2\pi f)^\alpha \mu_\alpha$
Maxwell	$\mu_1 \exp\left(-\dfrac{\mu_1}{\eta} t\right)$	$\dfrac{(i2\pi f)\eta}{1 + (i2\pi f)\dfrac{\eta}{\mu_1}}$
FD-Maxwell	$\mu_1 F_\alpha\left(-\dfrac{\mu_1}{\mu_\alpha} t^\alpha\right)$	$\dfrac{(i2\pi f)^\alpha \mu_\alpha}{1 + (i2\pi f)^\alpha \dfrac{\mu_\alpha}{\mu_1}}$
SL	$\dfrac{\mu_1\left(\mu_0 + \mu_1 e^{-\frac{(\mu_0+\mu_1)t}{\eta}}\right)}{\mu_0 + \mu_1}$	$\dfrac{\mu_0\mu_1 + \mu_1(i2\pi f)\eta}{\mu_0 + \mu_1 + (i2\pi f)\eta}$
FD-SL	$\dfrac{\mu_1\left(\mu_0 + \mu_1 F_\alpha\left(-\dfrac{(\mu_0+\mu_1)}{\mu_\alpha} t^\alpha\right)\right)}{\mu_0 + \mu_1}$	$\dfrac{\mu_0\mu_1 + \mu_1(i2\pi f)^\alpha \mu_\alpha}{\mu_0 + \mu_1 + (i2\pi f)^\alpha \mu_\alpha}$
SLS	$\mu_0 + \mu_1 e^{-\frac{\mu_1}{\eta}t}$	$\dfrac{\mu_0 + (i2\pi f)\eta \dfrac{(\mu_0+\mu_1)}{\mu_1}}{1 + (i2\pi f)\dfrac{\eta}{\mu_1}}$
FD-SLS	$\mu_0 + \mu_1 F_\alpha\left(-\dfrac{\mu_1}{\mu_\alpha} t^\alpha\right)$	$\dfrac{\mu_0 + (i2\pi f)^\alpha \mu_\alpha \dfrac{(\mu_0+\mu_1)}{\mu_1}}{1 + (i2\pi f)^\alpha \dfrac{\mu_\alpha}{\mu_1}}$

TABLE II
COMPARISON OF THE VISCOELASTIC PROPERTIES ESTIMATED USING THE SHEAR WAVE DISPERSION DATA OF PHANTOM

Model	μ_0 (Pa)	μ_1 (kPa)	η (Pas)	μ_α (Pas^α)	α
KV	13630	-	4.69	-	-
FD-KV	1.24e-10	-	-	456	0.52
Maxwell	-	28.01	14.42	-	-
FD-Maxwell	-	57.63	-	282.1	0.6
SL	1.01e+3	26.58	13.16	-	-
FD-SL	3.57e-9	400.94	-	733.1	0.43
SLS	1.00e+3	25.22	14.68	-	-
FD-SLS	54.73	355.93	-	352.1	0.55

TABLE III
MEDIAN (IQR) OF THE VISCOELASTIC PARAMETERS ESTIMATED USING SHEAR WAVE DISPERSION DATA OF PLANTAR SOFT TISSUE

Model	μ_0 (Pa)	μ_1 (kPa)	η (Pas)	μ_α ($kPas^\alpha$)	α
KV	13628.1 (13064.6 – 14902.8)	-	3.3 (2.9 – 3.8)	-	-
FD-KV	1e-11 (9e-12 – 24.99)	-	-	2.56 (0.94 – 4.64)	0.2684 (0.19 – 0.51)
Maxwell	-	21.7 (15.9 – 24.5)	17.8 (15.1 – 18.3)	-	-
FD-Maxwell	-	57.6 (37.8 – 119.7)	-	1.06 (0.86 – 2.00)	0.4 (0.37 – 0.48)
SL	30271.8 (29.39 – 20403.9)	25.2 (15.9 – 39.0)	15.1 (11.2 – 16.1)	-	-
FD-SL	48.57 (2.9e-4 – 799.0)	109.3 (88.1 – 476.2)	-	1.35 (0.79 – 2.64)	0.39 (0.27 – 0.44)
SLS	1.2e-5 (9.7e-6 – 14017.7)	15.6 (14.5 – 110.2)	15.7 (9.4 – 19.7)	-	-
FD-SLS	1.6 (0.5 – 3058.4)	310.0 (141.3 – 357.4)	-	1.98 (0.69 – 2.86)	0.29 (0.28 - 0.41)

References

Behforootan S, Chatzistergos P E, Chockalingam N and Naemi R 2017 A simulation of the viscoelastic behaviour of heel pad during weight-bearing activities of daily living *Annals of Biomedical Engineering* **45** 2750-61

Cavanagh P R, Ulbrecht J S and Caputo G M 2000 New developments in the biomechanics of the diabetic foot *Diabetes/metabolism research and reviews* **16** S6-S10

Chao C Y, Zheng Y P and Cheing G L 2011 Epidermal thickness and biomechanical properties of plantar tissues in diabetic foot *Ultrasound Med Biol* **37** 1029-38

Chen S, Fatemi M and Greenleaf J F 2004 Quantifying elasticity and viscosity from measurement of shear wave speed dispersion *The Journal of the Acoustical Society of America* **115** 2781-5

Craiem D, Rojo F, Atienza J, Guinea G and Armentano R L 2008 Fractional calculus applied to model arterial viscoelasticity *Latin American applied research* **38** 141-8

Hsu C C, Tsai W C, Wang C L, Pao S H, Shau Y W and Chuan Y S 2007 Microchambers and macrochambers in heel pads: are they functionally different? *J Appl Physiol (1985)* **103** 2227-31

Huang Y P and Zheng Y P 2015 *Measurement of Soft Tissue Elasticity in Vivo: Techniques and Applications*: CRC Press)

Jones D I G 2001 *Handbook of Viscoelastic Vibration Damping*: Wiley)

Kexue L and Jigen P 2011 Laplace transform and fractional differential equations *Applied Mathematics Letters* **24** 2019-23

Kiss M Z, Varghese T and Hall T J 2004 Viscoelastic characterization of in vitro canine tissue *Physics in Medicine & Biology* **49** 4207

Lin C-Y 2020 Alternative Form of Standard Linear Solid Model for Characterizing Stress Relaxation and Creep: Including a Novel Parameter for Quantifying the Ratio of Fluids to Solids of a Viscoelastic Solid *Frontiers in Materials* 7

Lin C-Y, Chen P-Y, Shau Y-W and Wang C-L 2017 An artifact in supersonic shear wave elastography *Ultrasound in medicine & biology* **43** 517-30

Miyake K, Yamakawa M, Kondo K, Namita T and Shiina T *2019 IEEE International Ultrasonics Symposium (IUS),2019-10-01 2019)*, vol. Series*)*: IEEE)

Murakami K, Tsukune M, Kobayashi Y, Fujie M, Kishimoto R, Obata T, Kawamura K, Yoshida K and Yamaguchi T *2015 IEEE International Ultrasonics Symposium (IUS),2015-10-01 2015)*, vol. Series*)*: IEEE)

Naemi R, Balasubramanian G, Darvel T and Chockalingam N 2021 Characteristics of patients with future diabetic foot ulceration. Can those be used to predict the ulceration incident? *Diabetic Medicine* **38**

Naemi R, Chatzistergos P, Suresh S, Sundar L, Chockalingam N and Ramachandran A 2017 Can plantar soft tissue mechanics enhance prognosis of diabetic foot ulcer? *Diabetes Res Clin Pract* **126** 182-91

Naemi R, Chatzistergos P E and Chockalingam N 2016 A mathematical method for quantifying in vivo mechanical behaviour of heel pad under dynamic load *Medical & biological engineering & computing* **54** 341-50

Naemi R and Chockalingam N 2013 Mathematical models to assess foot-ground interaction: an overview *Medicine and science in sports and exercise* **45** 1524-33

Naemi R, Romero Gutierrez S E, Allan D, Flores G, Ormaechea J, Gutierrez E, Casado-Pena J, Anyosa-Zavaleta S, Juarez M and Casado F 2022 Diabetes status is associated with plantar soft tissue stiffness measured using ultrasound reverberant shear wave elastography approach *Journal of Diabetes Science and Technology* **16** 478-90

Negishi T, Ito K, Kamono A, Lee T and Ogihara N 2020 Strain-rate dependence of viscous properties of the plantar soft tissue identified by a spherical indentation test *J Mech Behav Biomed Mater* **102** 103470

Ormachea J, Castaneda B and Parker K J 2018 Shear Wave Speed Estimation Using Reverberant Shear Wave Fields: Implementation and Feasibility Studies *Ultrasound Med Biol* **44** 963-77

Ormachea J, Lavarello R J, McAleavey S A, Parker K J and Castaneda B 2016 Shear Wave Speed Measurements Using Crawling Wave Sonoelastography and Single Tracking Location Shear Wave Elasticity Imaging for Tissue Characterization *IEEE Transactions on Ultrasonics, Ferroelectrics, and Frequency Control* **63** 1351-60

Ormachea J and Parker K J 2020 Elastography imaging: the 30 year perspective *Phys Med Biol* **65**

Ormachea J, Parker K J and Barr R G 2019 An initial study of complete 2D shear wave dispersion images using a reverberant shear wave field *Physics in Medicine & Biology* **64** 145009

Parker K J, Ormachea J, Drage M G, Kim H and Hah Z 2018 The biomechanics of simple steatosis and steatohepatitis *Phys Med Biol* **63** 105013

Parker K J, Ormachea J, Zvietcovich F and Castaneda B 2017 Reverberant shear wave fields and estimation of tissue properties *Physics in Medicine & Biology* **62** 1046

Parker K J, Szabo T and Holm S 2019 Towards a consensus on rheological models for elastography in soft tissues *Physics in Medicine & Biology* **64** 215012

Poul S S, Ormachea J, Ge G R and Parker K J 2022 Comprehensive experimental assessments of rheological models' performance in elastography of soft tissues *Acta Biomaterialia* **146** 259-73

Romero S E, Naemi R, Flores G, Allan D, Ormachea J, Gutierrez E, Casado F L and Castaneda B 2022 Plantar Soft Tissue Characterization Using Reverberant Shear Wave Elastography: A Proof-of-Concept Study *Ultrasound Med Biol* **48** 35-46

Roozbeh N, Sara B, Panagiotis C and Nachiappan C 2016 *Viscoelastic and Viscoplastic Materials*, ed E-A Mohamed Fathy (Rijeka: IntechOpen) p Ch. 10

Schmidt A and Gaul L 2008 Experimental investigation and numerical treatment of viscoelastic materials *Proceedings of the International Model Analysis Confernece* **3** 1557-66

Suzuki R, Ito K, Lee T and Ogihara N 2017 In-vivo viscous properties of the heel pad by stress-relaxation experiment based on a spherical indentation *Med Eng Phys* **50** 83-8

Zhang H, Zhang Q, Ruan L, Duan J, Wan M, Insana M F, Zhang H, Zhang Q, Ruan L, Duan J, Wan M and Insana M F 2018 Modeling Ramp-hold Indentation Measurements based on Kelvin-Voigt Fractional Derivative Model *Meas Sci Technol* **29**

Zhang M, Castaneda B, Wu Z, Nigwekar P, Joseph J V, Rubens D J and Parker K J 2007 Congruence of Imaging Estimators and Mechanical Measurements of Viscoelastic Properties of Soft Tissues *Ultrasound in Medicine & Biology* **33** 1617-31

Zhang W, Capilnasiu A and Nordsletten D 2021 Comparative analysis of nonlinear viscoelastic models across common biomechanical experiments *Journal of Elasticity* **145** 117-52

Zhang X, Kinnick R R, Pittelkow M R and Greenleaf J F *2008 IEEE Ultrasonics Symposium,2008-11-01 2008),* vol. Series*)*: IEEE)

Zhou B and Zhang X 2018 Comparison of five viscoelastic models for estimating viscoelastic parameters using ultrasound shear wave elastography *Journal of the mechanical behavior of biomedical materials* **85** 109-16

Zvietcovich F, Pongchalee P, Meemon P, Rolland J P and Parker K J 2019 Reverberant 3D optical coherence elastography maps the elasticity of individual corneal layers *Nature Communications* **10**

Zvietcovich F, Rolland J, Yao J, Meemon P and Parker K 2017 Comparative study of shear wave-based elastography techniques in optical coherence tomography *Journal of Biomedical Optics* **22** 035010